Enzyme and Microbial Technology 148 (2021) 109814

Contents lists available at ScienceDirect

Enzyme and Microbial Technology

journal homepage: www.elsevier.com/locate/enzmictec

Exploring the catalytic mechanism of a novel β-glucosidase BGL0224 from *Oenococcus oeni* SD-2a: Kinetics, spectroscopic and molecular simulation

Jie Zhang, Ning Zhao, Junnan Xu, Yiman Qi, Xinyuan Wei, Mingtao Fan *

College of Food Science and Engineering, Northwest A & F University, Yangling, Shaanxi, 712100, China

ARTICLE INFO

Keywords:
Amino acid
β-Glucosidase
Catalysis
Molecular docking
p-NPG
Food industry

ABSTRACT

The β-glucosidase derived from microorganisms has attracted worldwide interest for their industrial applications, but studies on β-glucosidases from *Oenococcus oeni* are rare. In this paper, catalytic mechanism of a novel β-glucosidase BGL0224 of *Oenococcus oeni* SD-2a was explored for the first time by kinetic parameters determination, fluorescence spectroscopy and quenching mechanism analysis, molecular dynamics simulation. The results indicated that BGL0224 had universal catalytic effect on different types of glycoside substrates, but the catalytic efficiencies were different. Fluorescence quenching analysis results suggested that the quenching processes between BGL0224 and seven kinds of substrates were predominated by the static quenching mechanism. A reasonable three-dimensional model of BGL0224 was obtained using the crystal structure of *E.coli* BglA as a template. The analysis results of molecular simulation (RMSD, Rg, RMSF and hydrogen bonding) showed that the composite system 'BGL0224-*p*NPG' was very stable after 40 ns. The catalytic process of BGL0224 acting on '*p*-Nitrophenyl β-D-glucopyranoside' conformed to the double displacement mechanism. Two glutamic acid residues 'Glu178 and Glu377' played a vital role in the whole catalytic process. Overall, this study gave specific insights on the catalytic mechanism of BGL0224, which was of great significance for developing its potential applications in food industry.

1. Introduction

As a kind of cellulase, β-glucosidase (EC3.2.1.21) is widely found in nature and it has been known for over 180 years since the first description of the action of emulsion (almond β-glucosidase) on amygdalin by Liebig and Wohler in 1837 [1]. Later researches indicated that β-glucosidase could be derived from plants, animals and microorganisms. The structure and enzymatic properties of β-glucosidase from different sources vary widely. The main function of β-glucosidase is to hydrolyze glycosidic bonds to release β-D-glucosyl residues [2]. There are two main classification methods for β-glucosidases [3,4]. Based on the amino acid sequences, β-glucosidases are classified as GH1, GH3, GH5, GH9, GH30 and GH116 families [5]. The other is based on substrate specificity. β-Glucosidases are categorized as aryl β-glucosidases, true cellobiases and wide range substrate specificity enzymes [6]. Among various β-glucosidase, microbial-derived β-glucosidase is attracting more industrial applications due to its advantages of large-scale preparation, inexpensive, and environment-friendly [7].

β-Glucosidase is vital for many biological processes. For example, it can promote biomass conversion. A thermotolerant β-glucosidase produced by the fungal strain BCC2871 (*Periconia* sp.) was found to possess the ability of hydrolyzing rice straw into simple sugars [8]. β-Glucosidase is also involved in the degradation of various functional glycoside precursors (e.g., terpenols, flavonoids and phytohormones) and potentially harmful metabolites (e.g., glycosylceramides) [9]. In addition, β-glucosidase is regarded as a versatile industrial biocatalyst. Compared to other industrial catalysts, β-glucosidase is significantly more stable and avoid enzyme subunit desorption [10]. Furthermore, β-glucosidase can hydrolyze many kinds of glycosides such as isoflavone glycosides and pyridoxine glucoside, which is very important to enhance the aroma profiles and quality of food products [11].

It is beneficial to study the catalytic mechanism of β-glucosidase and to improve the catalytic efficiency of cellulose hydrolysis. In recent years, many researchers were keen on exploring the molecular biology of β-glucosidase. For instance, Yang [12] revealed the distinct catalytic specificity and reaction kinetics of β-glucosidase (TN0602) through a combination of enzyme-substrate thermodynamic binding and molecular docking simulation. The three-dimensional model of the barley

* Corresponding author.
E-mail address: fanmt@nwsuaf.edu.cn (M. Fan).

https://doi.org/10.1016/j.enzmictec.2021.109814
Received 17 February 2021; Received in revised form 14 April 2021; Accepted 29 April 2021
Available online 3 May 2021

β-glucosidase gave an explanation not only for the enzyme's ability to hydrolyze some kinds of small, dimeric substrates but also for its preference for the relatively straight (1,4)-b-oligo glucoside substrates [13]. Pang [14] compared structures of the glucose-tolerant β-glucosidase 'Bgl6' and its variants at high resolution, which provided evidence for its glucose-tolerant mechanism and thermostability. From these reports we can see that detailed kinetic investigations and molecular simulation of essential residues have been much important for functional annotation of enzymes.

As a patented strain, *Oenococcus oeni* SD-2a plays a significant role in the process of wine fermentation, the most important reason is its high β-glucosidase activity. On the one hand, β-glucosidase can hydrolyze terpene glycosides and increase the aroma of wine. On the other hand, it has been proved to be related to the decomposition of anthocyanin glucosides, resulting color loss of wine in malolactic fermentation [15,16]. In all, studies on β-glucosidases from *Oenococcus oeni* focused more on the preliminary characterization and there were few reports on the catalytic mechanism. Therefore, in-depth study of the β-glucosidase of *O. oeni* SD-2a is necessary and of great significance. In our previous research, we have obtained a novel β-glucosidase BGL0224 of *Oenococcus oeni* SD-2a and its enzymatic properties were successfully characterized [17]. In this study, basic kinetics, spectroscopic and molecular simulation methods were applied to further understand the fundamental structure–function relationships and elucidate its catalytic mechanism, which is of great significance to develop its potential/performance as a commercial enzyme.

2. Materials and methods

2.1. Chemicals

All of the substrates with purity ≥99 % used in this study (*p*-Nitrophenyl β-D-glucopyranoside, *p*-Nitrophenyl β-D-galactopyranoside, *p*-Nitrophenyl β-D-xylopyranoside, *p*-Nitrophenyl β-D-cellobioside, *p*-Nitrophenyl β-D-glucuronide, *p*-Nitrophenyl α-D-glucopyranoside, *p*-Nitrophenyl α-D-galactopyranoside) were purchased from Yuanye Bio-Tech, Co., Ltd (Shanghai, China). Chemical structures of seven kinds of substrates were shown in Fig. S1. The remaining chemicals with purity ≥98 % were purchased from Solarbio Life-Science Co., Ltd (Beijing, China), which mainly included sodium chloride (NaCl), sodium carbonate (Na_2CO_3), potassium phosphate monobasic (KH_2PO4) and disodium phosphate (Na_2HPO_4). Water was purified by a Milli-Q Direct Water Purification System (Millipore, Billerica, MA).

2.2. Preparation of β-glucosidase BGL0224

O. oeni SD-2a was obtained from a Chinese wine region in Shandong province. The purified β-glucosidase BGL0224 belongs to glycoside hydrolase 1 (GH1) family and was expressed in our previous research [17]. Briefly, recombinant plasmid PcoldI-0224 was constructed and transformed into *E. coli* BL21 (DE3) for expression. Then, the crude enzyme solution was passed through a 'His·tag Ni-NTA Superflow Column' eluted with 300 mM imidazole and an ultrafiltration tube (30 kDa) to obtain the purified enzyme. The apparent molecular weight of BGL0224 is 55.15 kDa.

2.3. Enzyme activity assay

For all of the substrates, β-glucosidase activity was determined according to the method described by Dong [18] with slight modifications. Firstly, seven kinds of substrates were prepared at a concentration of 25 mM, respectively. Next, diluted and purified BGL0224 in 20 mM sodium phosphate buffer (pH 5.0) was incubated in 500 μL of reaction mixture containing 25 mM substrates, at 37℃ for 30 min. Then the reaction was terminated by adding 500 μL of 1 M Na_2CO_3, followed by measurement of the liberated *p*-nitrophenol (*p*-NP) at an absorbance of 420 nm. One unit of β-glucosidase activity was defined as the amount of enzyme that produces 1 μM of *p*-NP per min. β-Glucosidase activity was calculated according to the standard curve of *p*-NP ($Y = 0.0049X + 0.0185$, $R^2 = 0.9997$).

2.4. Effect of temperature and pH on enzyme activity

The purified β-glucosidase BGL0224 was dissolved in 20 mM sodium phosphate buffer (pH 5.0) to a final concentration of 10 mg/mL. 10 μL of the above solution was added to 490 μL solutions (25 mM) of seven substrates respectively. Then, 500 μL of the mixture was incubated at a temperature range of 25 ~ 70℃ for 30 min. 500 μL of 1 M Na_2CO_3 was added to the mixture to terminate the reaction. The β-glucosidase activities were measured according to the aforementioned method. The effects of pH on different substrates were determined at the optimal reaction temperature for each substrate. The purified enzyme BGL0224 was dissolved in 20 mM sodium phosphate buffer (pH 5.0) to a final concentration of 10 mg/mL. Simultaneously, seven substrates were dissolved in 20 mM sodium phosphate buffer with a pH range of 2.5 ~ 7.5. 10 μL of the enzyme solution was added to 490 μL of seven substrates solution (25 mM) with different pH respectively. Then, 500 μL of each mixture was incubated at the optimal reaction temperature for each substrate for 30 min. After that, 500 μL of 1 M Na_2CO_3 was added to each mixture to terminate the reaction. The β-glucosidase activities were measured according to the aforementioned method.

2.5. Determination of kinetic parameters of BGL0224

Enzyme kinetics parameters of BGL0224 acting on seven kinds of substrates were determined at the optimal reaction temperature and pH for each substrate. 100 μg of purified enzyme BGL0224 was added to various concentrations (0.1 ~ 25 mM) of each substrate. 500 μL of 1 M Na_2CO_3 was added to each mixture to terminate the reaction at 5 min. The Michaelis-Menten constant (K_m) and maximum rate of the reaction (V_{max}) were measured using nonlinear fitting of the Michaelis-Menten equation. Substrate concentrations were on the horizontal axis and the reaction rates were on the vertical axis. The'Hill'function (n = 1) in the OriginPro 8.0 software was used to fit the Michaelis-Menten equation. The turnover constant (K_{cat}) and the catalytic coefficient (ratio of K_{cat} to K_m) were then calculated.

2.6. Fluorescence spectra assays

Fluorescence evaluation was performed using a fluorescence spectrophotometer (PerkinElmer LS-55, Massachusetts, USA). The emission and excitation wavelengths of this assay were at 390 ~ 520 and 340 nm, respectively. The emission spectrum was measured from 390 to 520 nm in the presence of various concentrations (0 ~ 20 μM) of seven substrates by using 2.5 and 9 nm slit for excitation at the temperatures of 303 K. All measurements were carried out at enzyme concentration of 0.1 mg/mL and temperature of 303 K.

2.7. Homology modeling

The amino acid sequence of BGL0224 (GenBank accession number: MT330371) contained 480 amino acids. A BLAST search was performed against PDB (Protein Databank) using target sequence as a query to get the corresponding template for the protein BGL0224. For identification of suitable template, BLASTp was performed against PDB. An automated approach [19,20] of the MODELLER program was used to comparative protein structure modelling by satisfaction of spatial restraints and molecular mechanics. PROCHECK statistics and Verify 3D program were applied to evaluate the target model. Specifically, for PROCHECK, energy rules of stereochemical were used to judge the rationality of the protein model. The Verify 3D program mainly evaluated protein models by calculating the compatibility of a protein's 3D model with its own

amino acid sequence [21].

2.8. Molecular docking

Semi-flexible molecular docking method was applied to explore the catalytic mechanism of BGL0224 acting on '*p*-Nitrophenyl β-D-glucopyranoside'. The 3D structure of BGL0224 obtained by homology modeling was served as a receptor structure for molecular docking. Minimize the energy of the receptor structure to achieve a steady state. Then, the 3D structure of the substrate '*p*-Nitrophenyl β-D-glucopyranoside' was constructed by hydrogenation. The structure was optimized using the MOPAC program to calculate the atomic charge of PM3 [22,23]. Finally, Autodock Tools 1.5.6 were used to process the structure of the ligand and the receptor, respectively. The active sites were wrapped with docking box. The number of grid points in X, Y, Z directions was set to 60 × 60 × 60, the grid spacing was 0.375 Å, the number of docking times was 100, and the remaining parameters adopt default values [24].

2.9. Molecular dynamics simulation

In order to verify the stability of composite system 'BGL0224-*p*NPG', a 50 ns molecular dynamics (MD) simulation was performed on the structure of complex. The MD simulation was performed with 'Gromacs 2018' program [25], under constant temperature and constant pressure and periodic boundary conditions. Amber99SB full-atomic force field and TIP3P water model were used. In the process of MD simulation, all hydrogen bonds were constrained using the LINCS [26] algorithm, and the integration step was 2 fs. Electrostatic interactions were calculated using the Particle-mesh Ewald (PME) method [27]. The cutoff value of non-bonded interaction was set to 10 Å and updated every 10 steps. The 'V-rescale' temperature coupling method [28] and the 'Parrinello-Rahman' method [29] were used to control the simulated temperature and pressure to 300 K and 1 bar, respectively. The steepest descent method was applied to minimize the energy of the system to eliminate close contacts between atoms. 100 ps NVT equilibrium simulation was performed at 300 K and the MD simulation of the composite system was performed at 50 ns. Visualization of simulation results were done using Gromacs embedded program and Visual Molecular Dynamics (VMD).

3. Results

3.1. Investigation of substrate specificity

The effects of different temperatures and pH on BGL0224 catalyzing seven kinds of substrates were shown in Fig. 1. On the whole, BGL0224 had the strongest catalytic effect on '*p*-Nitrophenyl β-D-glucopyranoside', followed by '*p*-Nitrophenyl β-D-cellobioside', '*p*-Nitrophenyl β-D-galactopyranoside' and '*p*-Nitrophenyl β-D-xylopyranoside'. In the seven reactions, the optimal temperatures for catalyzing '*p*-Nitrophenyl β-D-xylopyranoside' and '*p*-Nitrophenyl β-D-glucuronide' were 40℃ and 45℃ respectively, and the optimal temperatures for catalyzing the other five substrates were 50℃. Fig. 1c and d showed that the optimal pH of BGL0224 catalyzing seven kinds of substrates were all 5.0 and the enzyme activity of BGL0224 was significantly reduced when the pH value was greater than 6.0. The kinetic parameters of BGL0224 acting on seven kinds of substrates were shown in Table 1. When catalyzing the substrate containing 'β-' bonds, the values of V_{max} were generally larger except '*p*-Nitrophenyl β-D-glucuronide' and the maximum V_{max} value was 382.81 U/mg. The K_m value is usually used to measure the affinity between enzyme and substrate. Smaller K_m value indicates greater affinity between enzyme and substrate. BGL02024 had the smallest K_m value when catalyzing the substrate '*p*-Nitrophenyl β-D-glucopyranoside', which was 0.34 μM. The ratio of K_{cat} to K_m is an important parameter for measuring the catalytic efficiency of enzymes and can be used to determine the optimal substrate for enzyme. As it was shown in Table 1, the best substrate for hydrolysis by BGL0224 was '*p*-Nitrophenyl β-D-glucopyranoside' and the ratio of K_{cat} to K_m was 1034.94 S^{-1}/μM.

3.2. Fluorescence spectroscopy and quenching mechanism

Took '*p*-Nitrophenyl β-D-glucopyranoside' as an example, the effects of different concentrations of '*p*-Nitrophenyl β-D-glucopyranoside' on the fluorescence intensity of BGL0224 were shown in Fig. 2a. BGL0224 had the strongest fluorescence intensity with a emission wavelength at 439 nm. When '*p*-Nitrophenyl β-D-glucopyranoside' was added to the

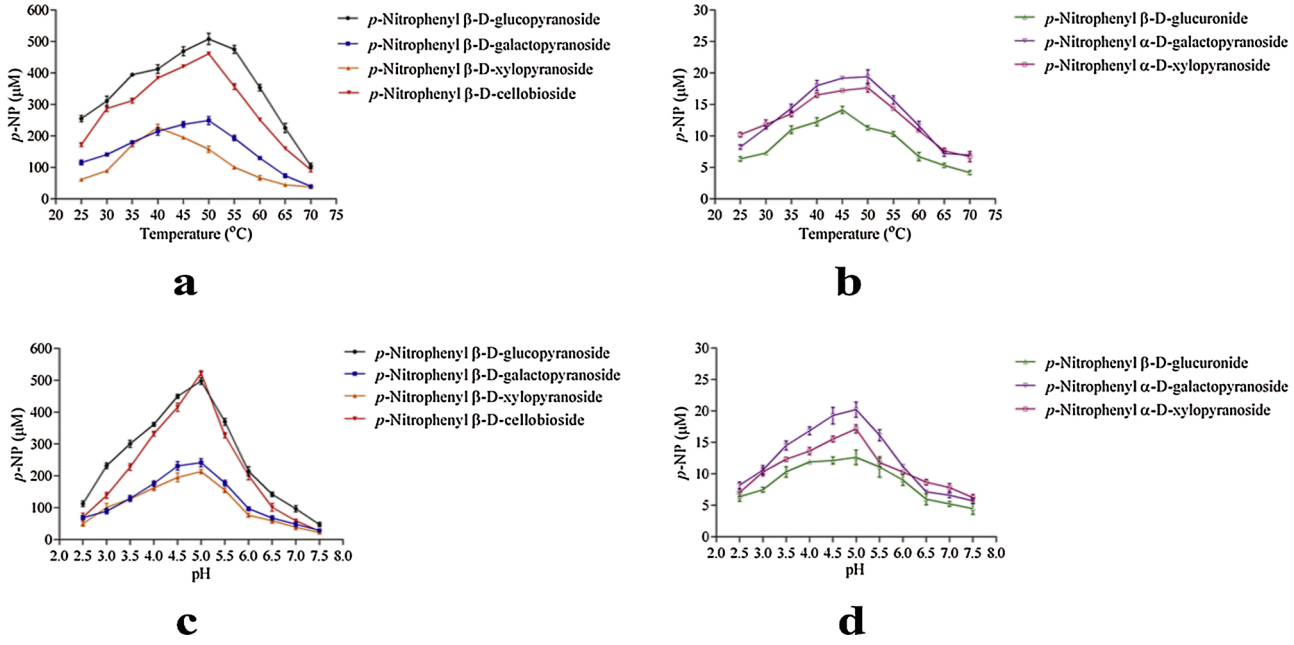

Fig. 1. Effect of different temperatures and pH on BGL0224 catalyzing seven kinds of substrates. a, b: Effect of temperature on the activity of BGL0224 catalyzing seven kinds of substrates. c, d: Effect of pH on the activity of BGL0224 catalyzing seven kinds of substrates. Vertical bars show the standard deviations of three replicates.

Table 1
Kinetic parameters of BGL0224 catalyzing seven kinds of substrates.

Substrates	V_{max} (U/mg)	K_m (μM)	K_{cat} (S^{-1})	K_{cat}/K_m (S^{-1}/μM)
p-Nitrophenyl β-D-glucopyranoside	382.81 ± 7.76	0.34 ± 0.04	351.88 ± 7.13	1034.94
p-Nitrophenyl β-D-galactopyranoside	270.88 ± 6.86	0.95 ± 0.13	248.99 ± 6.30	262.09
p-Nitrophenyl β-D-xylopyranoside	256.43 ± 6.13	1.10 ± 0.14	235.71 ± 5.63	214.28
p-Nitrophenyl β-D-cellobioside	359.54 ± 5.55	0.43 ± 0.04	330.49 ± 5.10	768.58
p-Nitrophenyl β-D-glucuronide	24.17 ± 1.63	1.87 ± 0.58	22.21 ± 1.50	11.88
p-Nitrophenyl α-D-glucopyranoside	39.27 ± 1.51	1.42 ± 0.26	36.10 ± 1.39	25.42
p-Nitrophenyl α-D-galactopyranoside	39.64 ± 1.02	1.70 ± 0.20	36.43 ± 0.94	21.43

Values represent means ± standard error (n = 3).

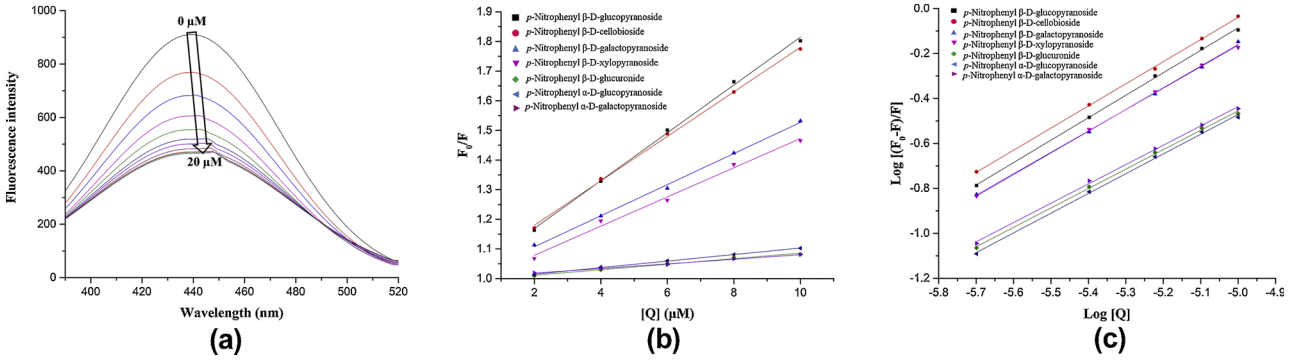

Fig. 2. Fluorescence quenching analysis of BGL0224. a: Fluorescence spectra of BGL0224 in the absence and presence of different concentrations of '*p*-Nitrophenyl β-D-glucopyranoside' at 303 K. b: The Stern-Volmer plot of BGL0224 quenching by various concentrations of substrates at 303 K. c: Double logarithmic plot of BGL0224 quenching by various concentrations of substrates at 303 K.

solution of BGL0224, the intrinsic fluorescence intensity of BGL0224 was decreased gradually and regularly. In addition, with the increasing of substrate concentration, a red shift of the peak (from 439 nm to 448 nm) was observed. The fluorescence quenching process was described and calculated with the following Stern-Volmer equation [30] and the results were shown in Table 2 and Fig. 2b.

$$\frac{F_0}{F} = 1 + K_{SV}[Q] = 1 + K_q\tau_0[Q] \quad (1)$$

where F_0 and F are the fluorescence intensities of BGL0224 in the absence and presence of substrates; [Q] are concentration of substrates; τ_0 denotes the average lifetime of the fluorophore in the absence of the quencher ($\tau_0 = 1 \times 10^{-8}$ s), K_{SV} and K_q mean the Stern-Volmer quenching constant and the quenching rate constant, respectively. The calculation results indicated that when seven kinds of substrates were added to the enzyme solution, the K_{SV} of BGL0224 were 8.07 × 10^4, 5.25 × 10^4, 4.93 × 10^4, 7.51 × 10^4, 0.93 × 10^4, 1.10 × 10^4 and 0.78 × 10^4 L·M^{-1}, respectively. In addition, the values of K_q were all much greater than 2.0 × 10^{10} L·M^1·s^{-1}, suggesting that the fluorescence quenching processes were predominated by the static quenching mechanism rather than the dynamic [31]. Then, the fluorescence quenching data were further calculated with the following equation [30].

$$log\frac{F_0 - F}{F} = log\ K_b + nlog[Q] \quad (2)$$

where F_0 and F are the fluorescence intensities of BGL0224 in the absence and presence of substrates; [Q] are concentration of substrates; K_b is the binding constant, n denotes the number of the binding sites. The plots of log [$(F_0 - F)/F$] versus log [Q] were presented in Fig. 2c, and the results were shown in Table 2. The values of n were all approximately equal to 1, which indicated that there was only one binding site on the enzyme for each substrate. The binding constants between BGL0224 and seven kinds of substrates were 8.09 × 10^4, 4.53 × 10^4, 3.94 × 10^4, 7.62 × 10^4, 0.73 × 10^4, 0.83 × 10^4 and 0.73 × 10^4 L·M^{-1}, respectively.

Table 2
Quenching and binding parameters of BGL0224-substrates complex.

Substrates	K_{sv} (L·M^{-1}) x 10^4	K_q (L·$M^{-1}$$S^{-1}$) x 10^{12}	K_b (L·M^{-1}) x 10^4	n
p-Nitrophenyl β-D-glucopyranoside	8.07	8.07	8.09	0.99
p-Nitrophenyl β-D-galactopyranoside	5.25	5.25	4.53	0.98
p-Nitrophenyl β-D-xylopyranoside	4.93	4.93	3.94	0.95
p-Nitrophenyl β-D-cellobioside	7.51	7.51	7.62	0.96
p-Nitrophenyl β-D-glucuronide	0.93	0.93	0.73	0.86
p-Nitrophenyl α-D-glucopyranoside	1.10	1.10	0.83	0.88
p-Nitrophenyl α-D-galactopyranoside	0.78	0.78	0.73	0.86

K_{sv} is the Stern–Volmer quenching constant and K_q is quenching rate constant. K_b is binding constant and n is the number of binding sites.

3.3. Homology modeling

By searching the PDB database, it was found that the crystal structure of *E.coli* BglA (ID: 2XHY) [32] had high sequence identity with β-glucosidase BGL0224. The exact sequence alignment results were shown in Fig. 3. Generally, the known crystal structure could be used as a template for homology modeling when the sequence identity between the crystal structure and the target protein was more than 30 %. In this research, the identity of the two sequences reached 57 %. Therefore, the crystal structure of 2XHY was a very good template for homology modeling. The results of the homology modeling and the rationality evaluation were shown in Fig. 4. The rationality evaluation of protein model by PROCHECK program was expressed in the form of 'Ramachandran plot' which could be used to illustrate the rotation of the bond between α carbon atom and the carbonyl carbon atom to the

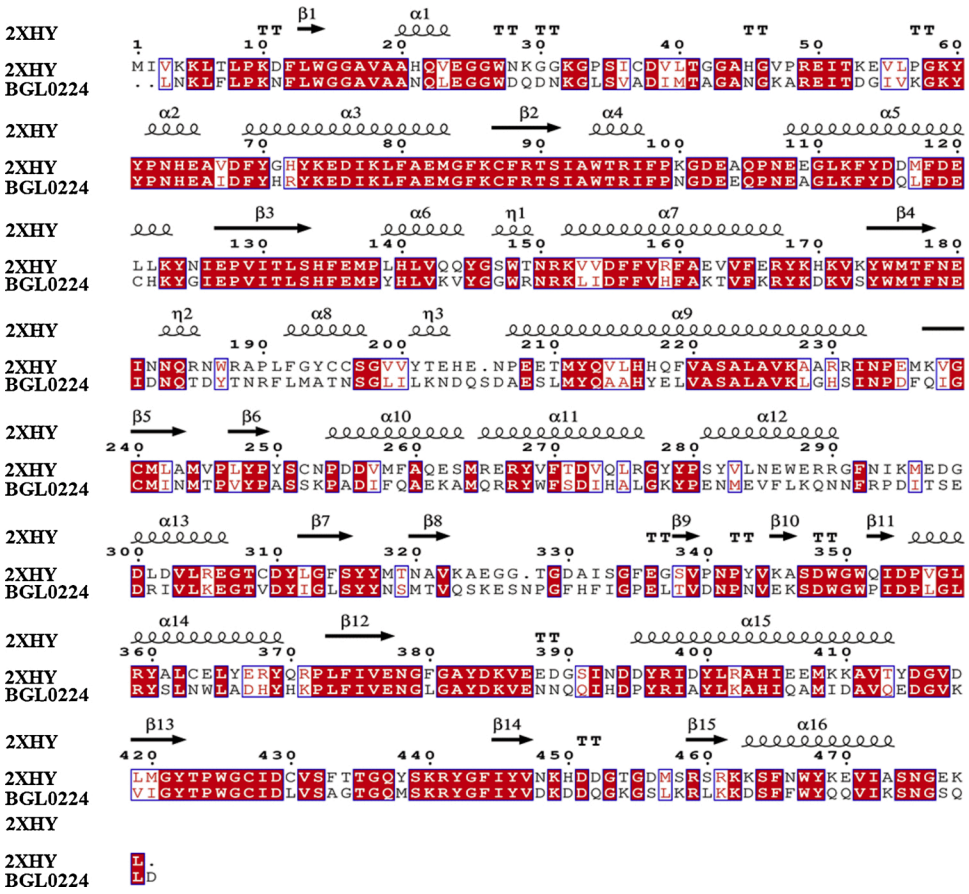

Fig. 3. Sequence alignment of 2XHY and BGL0224. Similar sequences are marked by boxes and identical sequences are highlighted in red.

rotation between α carbon atom and the nitrogen atom bond within the three-dimensional structure of protein. The 'Ramachandran plot' in Fig. 4a was divided into three regions: the allowable region (red color), the maximum allowable region (yellow color), and the prohibition region (blank). The amino acid residues in the allowable region reached 90.14 %. Only 0.20 % of the amino acid residues were in the prohibition region, and the remaining 99.80 % were in a reasonable range, which conformed to the energy rules of stereochemistry [33]. The compatibility of BGL0224's 3D model with its own amino acid sequence was mainly evaluated by the Verify 3D program. The Verify 3D score of the protein model was shown in Fig. 4b. 95.99 % of the amino acid residues scored above 0.2, which met the requirements of the evaluation program. According to 'Ramachandran plot' and Verify 3D score, the 3D structure illustrated in Fig. 4d was reasonable and could be used as a template for subsequent research. The flexibility of amino acids in the protein structure can be expressed by RMSF (Root Mean Square Fluctuation). The RMSF distribution of α carbon atoms in amino acid residue in the structure were shown in Fig. 4c. The RMSF values of most amino acids were below 0.2, indicating that the overall flexibility of BGL0224 was relatively low.

3.4. Molecular dynamics analysis

The aforementioned results indicated that the best substrate for hydrolysis by BGL0224 was '*p*-Nitrophenyl β-D-glucopyranoside'. Therefore, in this section, '*p*-Nitrophenyl β-D-glucopyranoside' was used as the substrate to explore the catalytic mechanism of BGL0224. The enzyme-substrate composite system 'BGL0224-*p*NPG' was obtained by semi-flexible molecular docking. The stability of the composite system can be obtained by analyzing the convergence parameters during the simulation. The convergence parameters mainly include the RMSD (Root Mean Square Deviation) and Rg (Radius of Gyration) [34]. RMSD means the sum of all atomic deviations between the conformation at a certain moment and the target conformation, and it is an important basis for measuring whether the system is stable. The RMSD results of the main chain atoms of the composite system within 50 ns were shown in Fig. 5a. It can be seen from the figure that the composite system basically reached a steady state after 40 ns, and the RMSD value of the stable system was 0.223 ± 0.016 nm. Rg can be used to describe changes of the composite system. The greater change of Rg means the greater expansion of the system. As it was shown in Fig. 5b, due to the solvation of the compound during the simulation progress, the Rg value of the composite system gradually increased until it stabilized at 40 ns. The Rg value of the stable system was 2.204 ± 0.006 nm.

The number of hydrogen bonds inside the BGL0224 (Fig. 5c) and the hydrogen bonds between the BGL0224 and the substrate (Fig. 5d) were separately counted during the MD simulation. It can be seen from the two figures that the number of hydrogen bonds inside the BGL0224 was basically stable at about 360 during the MD simulation, while the number of hydrogen bonds between the BGL0224 and the substrate tended to be stable at 40 ns, about 4. The number of hydrogen bonds remained stable during the MD simulation, indicating that the structure of the composite system did not change significantly. In addition, according to the MD simulation trajectory, the binding energy of the composite system was calculated (Fig. 5e). The binding energy was mainly composed of Coulomb energy and LJ energy. The contribution of the two energies to the binding energy was basically the same. The binding energy of the composite system fluctuated greatly in the first 20 ns, and gradually stabilized after 40 ns, with a value of -202.00 ± 20.72 kJ/mol.

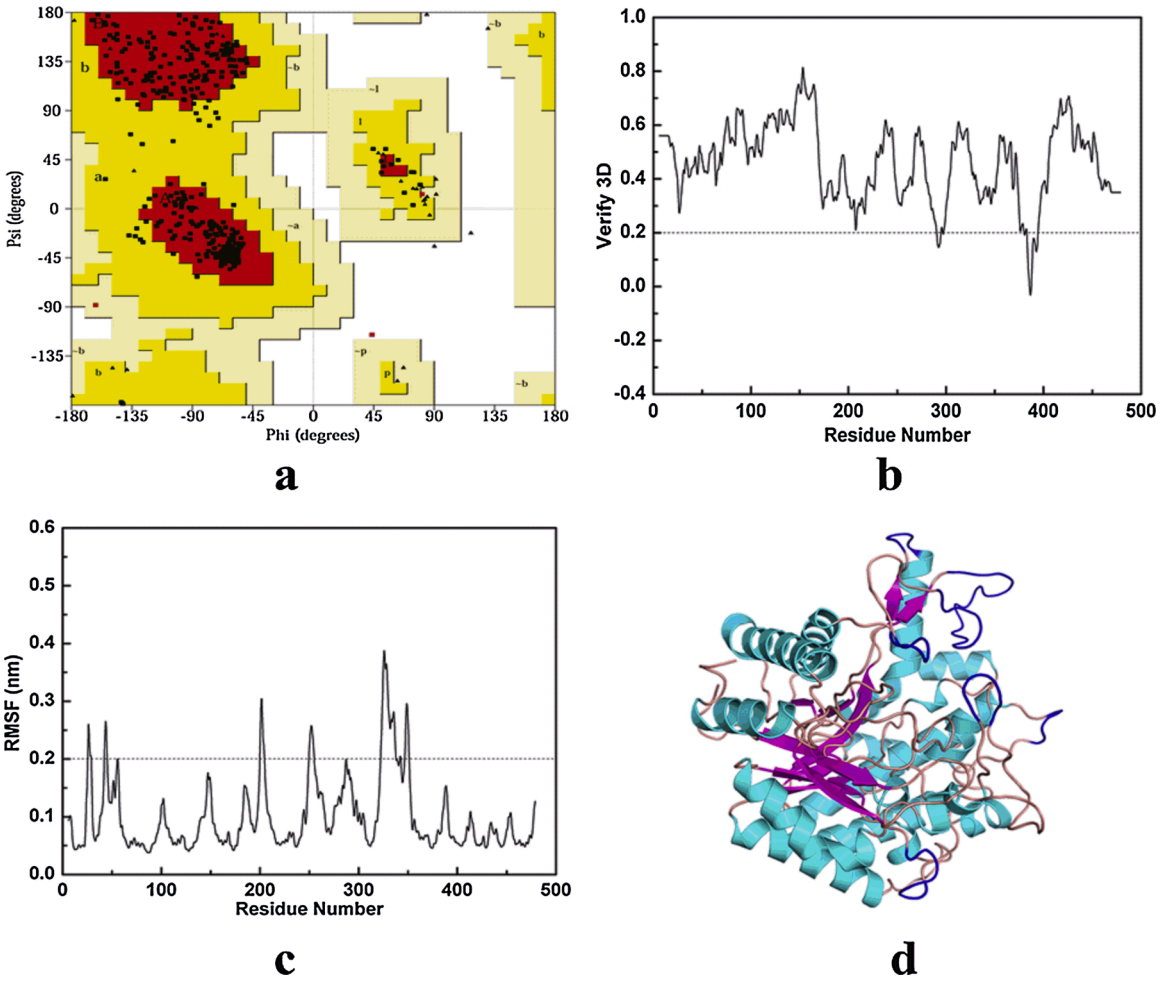

Fig. 4. Model construction and verification of BGL0224. a: 'Ramachandran plot' of modeled BGL0224 protein. b: Verify 3D score profile of modeled BGL0224 protein. c: The RMSF distribution of α carbon of amino acid residues in the structure of BGL0224. d: 3D structure of BGL0224, where cyan represented the alpha helices, purple represented the beta sheets, and blue lines represented the areas of greater flexibility.

3.5. Binding mode and catalytic mechanism

In order to further understand the interaction between BGL0224 and *p*-NPG, the structure of composite system 'BGL0224-*p*NPG' after MD simulation was extracted and the binding mode was analyzed in detail (Fig. 6a). The hydrophilic amino acids of the active pocket of BGL0224 were the main part of the binding process. These hydrophilic amino acids mainly included Gln20, His132, Glu178 and Glu377. The sugar moiety of the substrate was combined with hydrophilic amino acids and formed hydrogen bonds with these amino acid residues, which played an important role in stabilizing the glycosyl structure of the substrate to maintain a relatively stable conformation during the catalytic process. At the same time, in the vicinity of the three amino acid residues Tyr316, Trp351 and Tyr442 with aromatic ring side chains, a strong π-π interaction could be formed between the nitrophenyl groups of the substrate, and the nitro group also formed hydrogen bonds with Asn317, which further limited the conformational changes of substrate. Therefore, hydrogen bonding and π-π interaction were important driving force for the combination of BGL0224 and *p*-NPG. The reaction process of β-glucosidase BGL0224 hydrolyzed the glycosidic bond to generate glucose and the corresponding ligand as shown in Fig. 6b: firstly, the substrate *p*-NPG bound to the catalytic active site of BGL0224. The carbonyl oxygen atom of Glu377 attacked the C atom of the substrate, thereby breaking the glycosidic bond. The oxygen atom of the ligand captured the hydrogen atom of Glu178 to form a *p*-Nitrophenol and then the *p*-Nitrophenol was removed. After that, water molecules entered the active center of BGL0224. The hydrogen atom of water molecules bound to the carboxyl group of Glu178, and the remaining hydroxide anions bound to glucose, breaking the covalent bond between glucose and Glu377 to generate the final product glucose.

4. Discussion

This study explored the fundamental structure–function relationships of a novel β-glucosidase BGL0224 from *Oenococcus oeni* SD-2a and elucidated its catalytic mechanism. Based on the present work, the catalytic effect on seven kinds of substrates, fluorescence quenching, homology modeling, molecular dynamics analysis, binding mode and catalytic mechanism of BGL0224 have been carried out.

BGL0224 had catalytic effects on all seven kinds of substrates, at the same time, it had strong steroslectivity. When catalyzing seven kinds of substrates, the effect of acid and heat on the catalytic ability of BGL0224 was similar to other reported β-glucosidases. For example, the higher optimum catalytic temperature indicated that BGL0224 was a thermostable enzyme, which was consistent with most of the reported GH1 β-glucosidases [35,36]. In addition, enzymes are typically pH sensitive due to the need to maintain keep catalytic groups in the correct ionization state. Here, catalytic glutamate needs to function as a general acid and high pHs could destabilize the protonated residue and impede catalytic reaction. Therefore, BGL0224 showed acidic pH optima. Generally, the pH value of wine is around 3.5. The preference of β-glucosidase BGL0224 for acidic environment had undoubtedly broadened its

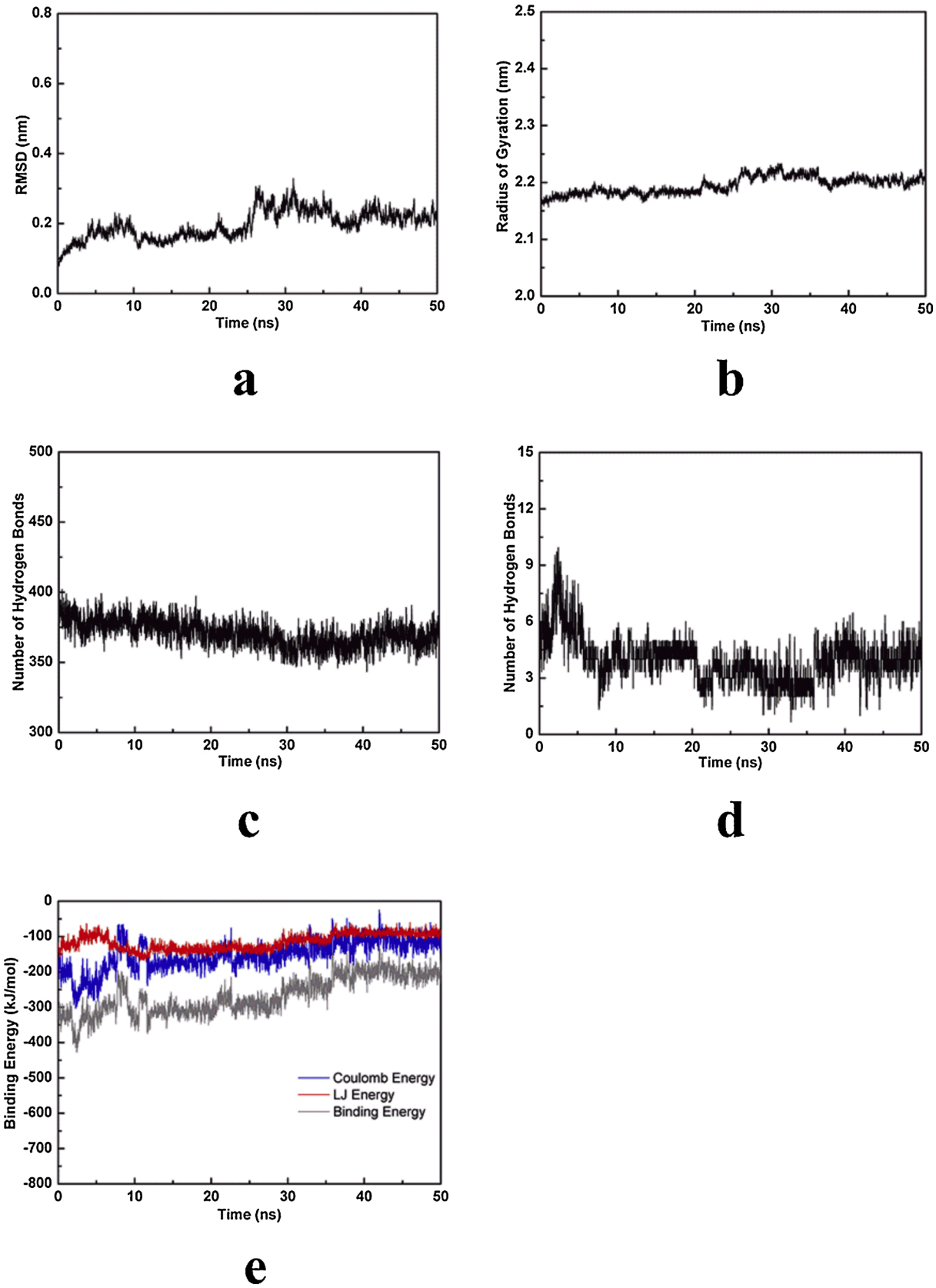

Fig. 5. Molecular dynamics simulation of BGL0224 catalyzing *p*-NPG. a: Variation of RMSD of the composite system 'BGL0224-*p*NPG' during MD simulation. b: Variation of Rg of the composite system 'BGL0224-*p*NPG' during MD simulation. c: Variation of hydrogen bonds within BGL0224 during MD simulation. d: Variation of hydrogen bonds between BGL0224 and *p*-NPG during MD simulation. e: Variation of binging energy of the composite system 'BGL0224-*p*NPG' during MD simulation.

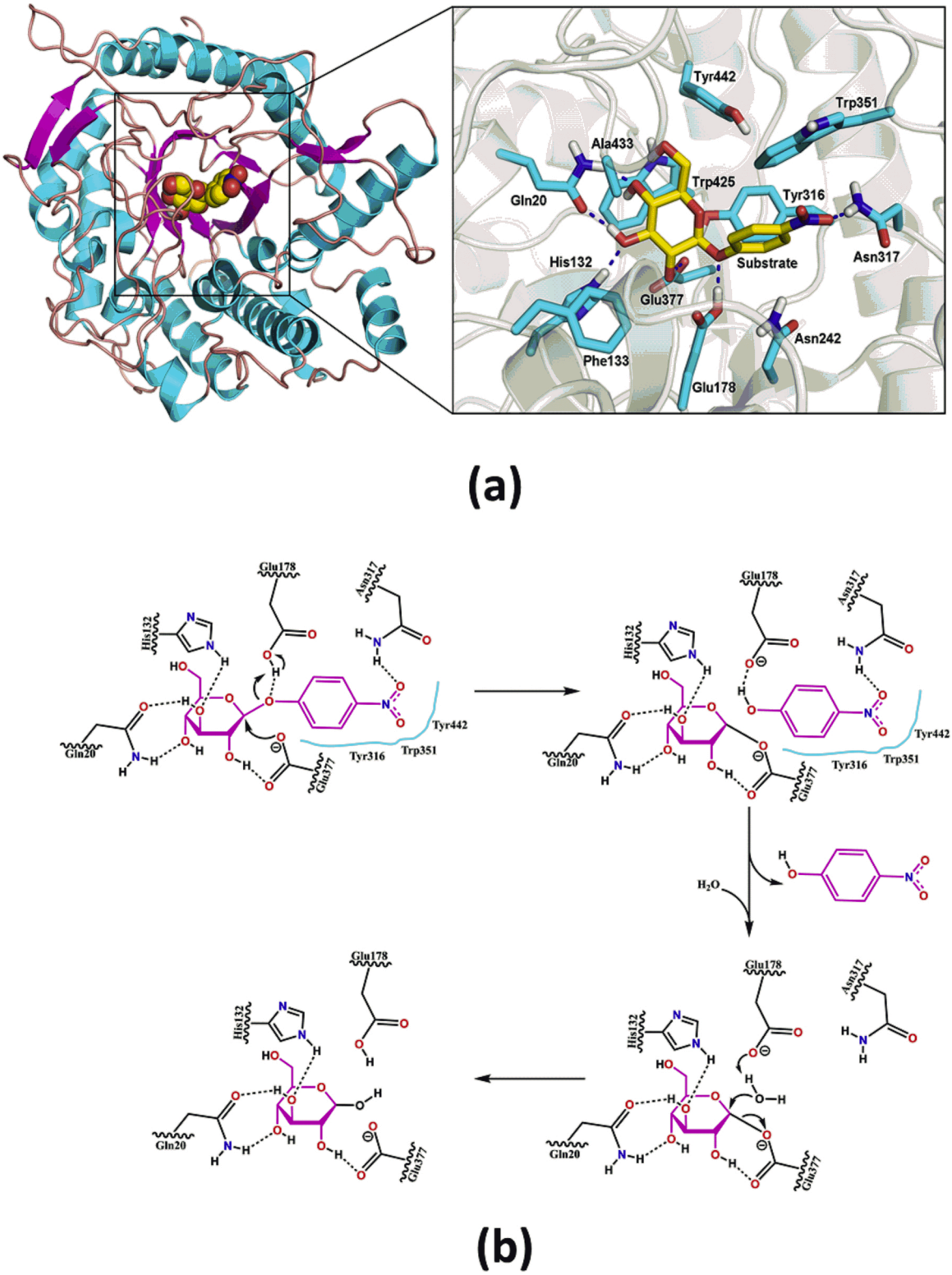

Fig. 6. Binding mode and catalytic mechanism of BGL0224. a: Diagram of the binding mode of BGL0224 and *p*-NPG. b: Catalytic mechanism of BGL0224 acting on *p*-NPG. Dashed line indicates hydrogen bonds, blue curve indicates hydrophobic interaction.

application in the wine industry. In addition, β-glucosidase BGL0224 had a stronger catalytic effect on substrates containing 'β-' bonds, and a weaker catalytic effect on substrates containing 'α-' bonds. Specifically, among the seven kinds of substrates, β-glucosidase BGL0224 had the highest affinity for substrate '*p*-Nitrophenyl β-D-glucopyranoside' and the lowest affinity for substrate '*p*-Nitrophenyl β-D-glucuronide'. According to some recent reports, both the sugar moiety and the type of glycosidic linkage were essential to substrate recognition [37,38]. It was also reflected in this study. Although BGL0224 had general catalytic effects on 'β-' bonds, different ligands could also affect the catalytic efficiency. The low catalytic efficiency of BGL0224 for substrate '*p*-Nitrophenyl β-D-glucuronide' proved this. Clearly, BGL0224 had a

strong catalytic effect on substrates containing 'β-' bonds except when the substituent was glucuronide. In contrast, it had a weak catalytic effect on substrates containing 'α-' bonds, indicating the substrate specificity of BGL0224.

The binding between the seven kinds of substrates and BGL0224 followed a static quenching mechanism, and the binding site was predicted to be one. The fluorescent properties of protein are mainly related to whether it contains amino acid residues with fluorescent properties. Amino acid residues with endogenous fluorescence properties mainly include tryptophan (Trp), tyrosine (Tyr) and phenylalanine (Phe). Sequence analysis of BGL0224 indicated that its amino acid sequence contained a total of 28 Tyr residues, 27 Phe residues and 11 Trp residues, accounting for 5.83 %, 5.63 % and 2.29 % of total number of amino acid residues, respectively. Therefore, the quenching mechanism can be explored by measuring the emission spectrum of BGL0224 with different concentrations of substrates. Fluorescence quenching is the decrease in the quantum yield of fluorescence from a fluorophore induced by a variety of molecular interactions with quencher molecules [39,40]. Therefore, examination of small molecule induced quenching of a protein can determine the binding mechanism. In this study, the gradual and regular decrease in the fluorescence intensity of BGL0224 indicated that the conformational changes of the enzyme during the reaction process. The red shift of the peak in Fig. 2a suggested that '*p*-Nitrophenyl β-D-glucopyranoside' quenched the intrinsic fluorescence of BGL0224 and increased the polarity of the fluorophore microenvironments [41]. These findings suggested that there were interactions and strong affinity between BGL0224 and seven kinds of substrates, especially for the substrate '*p*-Nitrophenyl β-D-glucopyranoside' and '*p*-Nitrophenyl β-D-cellobioside', which was similar to the results of 'substrate specificity' section.

The evaluation results showed that the 3D structure of BGL0224 constructed with the crystal structure of 2XHY as a model possessed good stability. Fig. 4d showed the overall structure of BGL0224. There was a $(\beta/\alpha)_8$-barrel domains that contained the active site. It was somewhat different from the double-barrel structure of GH3 β-glucosidase in some plants [42]. And the overall structure of BGL0224 exhibited low flexibility. The main reason was that the middle β-sheets were wrapped by more α-helices and the overall structure was relatively stable. In addition, amino acids with greater flexibility were mainly distributed in Gly24 ~ Asn29, Ala42 ~ Ala46, Lys200 ~ Ser204, Ser250 ~ Ala254, Ser323 ~ Val339, Ser347 ~ Trp351 regions, which are located in the 'loop' region of BGL0224's 3D structure. The 'loop' region was exposed to water environment and had a strong interaction with the surrounding water molecules, so its flexibility was greater than other regions.

Catalytic reaction process of BGL0224 acting on *p*-NPG conformed to double displacement mechanism. There are four types of non-covalent inter-actions that could play a key role in ligand binding to proteins: hydrogen bonds, van der Waals forces, electrostatic forces and hydrophobic bonds interactions. In this study, hydrogen bonding was considered to be the most important non-covalent inter-actions to maintain the high-level structural stability of BGL0224. By analyzing the convergence parameters in the simulation process, it was found that the composite system tends to be stable after 40 ns. Compared to some other reported complex [43,44], 'BGL0224-*p*NPG' possessed a relatively low binding energy, indicating that the composite system 'BGL0224-*p*NPG' was very stable. According to the speculation of Li [45] and Guce [46], the hydrolysis action of β-glucosidase mainly depended on the two carboxyl-carrying amino acids (glutamic acid and aspartic acid) which near the glycosidic bond. In this paper, the corresponding amino acid residues with catalytic functions also existed around the substrate in the composite structure. The catalytic reaction process conformed to the double displacement mechanism and it can be seen that the two glutamic acid residues 'Glu178 and Glu377' play a vital role in the whole catalytic process. This provided a theoretical basis for the subsequent molecular modification of the β-glucosidase. We hope that the structural information will be used to engineer the enzyme for enhancing its catalytic efficiency and further apply it to industrial production.

5. Conclusion

In conclusion, higher catalytic temperature and lower pH value were more suitable for BGL0224. On the one hand, BGL0224 had catalytic effects on all seven kinds of substrates, especially for substrates containing 'β-' bonds. On the other hand, it showed somewhat substrate selectivity. '*p*-Nitrophenyl β-D-glucopyranoside' was considered to be the most suitable substrate, which is similar to the result of fluorescence quenching analysis. The homology modeling and subsequent verification results showed that the three-dimensional structure of BGL0224 conformed to the energy rules of stereochemical. The MD simulation results for complex 'BGL0224-*p*NPG' indicated that its overall conformation stabilized at 40 ns. Two glutamic acid residues 'Glu178 and Glu377' were the core of catalytic process. Overall, this study gave specific insights on the catalytic mechanism of BGL0224, which offered theoretical basis for its industrial application.

Funding

This work was supported by the grant of National Natural Science Foundation of China (31871769).

CRediT authorship contribution statement

Jie Zhang: Conceptualization, Investigation, Data curation, Writing - original draft. **Ning Zhao:** Investigation. **Junnan Xu:** Software, Data curation. **Yiman Qi:** Conceptualization. **Xinyuan Wei:** Writing - review & editing. **Mingtao Fan:** Conceptualization, Supervision, Writing - review & editing.

Declaration of Competing Interest

The authors report no declarations of interest.

Appendix A. Supplementary data

Supplementary material related to this article can be found, in the online version, at doi:https://doi.org/10.1016/j.enzmictec.2021.109814.

References

[1] A. Esen, β-Glucosidases : overview, Biochem. Mol. Biol. 533 (1993) 1–14, https://doi.org/10.1021/bk-1993-0533.
[2] D.L. Zechel, S.G. Withers, Glycosidase mechanisms: anatomy of a finely tuned catalyst, Acc. Chem. Res. 33 (2000) 11–18, https://doi.org/10.1021/ar970172+.
[3] T.C. Bhalla, M. Asif, K. Smita, Purification and characterization of cyanogenic β-glucosidase from wild apricot (*Prunus armeniaca* L.), Process. Biochem. 58 (2017) 320–325, https://doi.org/10.1016/j.procbio.2017.04.023.
[4] A.U. Cristiane, T. Gaku, W. Hirofumi, K. Katsuhiko, A. Manabu, A novel glucose-tolerant β-glucosidase from the salivary gland of the termite *Nasutitermes takasagoensis*, J. Gen. Appl. Microbiol. 59 (2013) 141–145, https://doi.org/10.2323/jgam.59.141.
[5] J.R.K. Cairns, A. Esen, β-Glucosidases, Cell. Mol. Life Sci. 67 (2010) 3389–3405, https://doi.org/10.1007/s00018-010-0399-2.
[6] E.J. Hwang, Y.S. Lee, Y.L. Choi, Cloning, purification, and characterization of the organic solvent tolerant β -glucosidase, OaBGL84, from *Olleya aquimaris* DAU311, Appl. Biol. Chem. 61 (2018) 1–12, https://doi.org/10.1007/s13765-018-0361-9.
[7] D. Sternberg, P. Vuayakumar, E.T. Reese, β-Glucosidase: microbial production and effect on enzymatic hydrolysis of cellulose, Can. J. Microbiol. 23 (1977) 139–147, https://doi.org/10.1139/m77-020.
[8] P. Harnpicharnchai, V. Champreda, W. Sornlake, L.L. Eurwilaichitr, A thermotolerant β-glucosidase isolated from an endophytic fungi, *Periconia* sp., with a possible use for biomass conversion to sugars, Protein Expr. Purif. 67 (2009) 61–69, https://doi.org/10.1016/j.pep.2008.05.022.
[9] Y. Bhatia, S. Mishra, V.S. Bisaria, Microbial β-glucosidases: cloning, properties, and applications, Crit. Rev. Biotechnol. 22 (2002) 375–407, https://doi.org/10.1080/07388550290789568.

[10] P.G. Vazquez-Ortega, M.T. Alcaraz-Fructuoso, J.A. Rojas-Contreras, J. López-Miranda, R. Fernandez-Lafuente, Stabilization of dimeric β-glucosidase from *Aspergillus niger* via glutaraldehyde immobilization under different conditions, Enzyme Microb. Technol. 110 (2018) 38–45, https://doi.org/10.1016/j.enzmictec.2017.12.007.

[11] P. Vernocchi, F. Patrignani, M. Ndagijimana, C.C. Lopez, G. Suzzi, F. Gardini, R. Lanciotti, Trebbiano wine produced by using *Saccharomyces cerevisiae* strains endowed with β-glucosidase activity, Ann. Microbiol. 65 (2015) 1565–1571, https://doi.org/10.1007/s13213-014-0995-8.

[12] J. Yang, R. Gao, Y. Zhou, S. Anankanbil, J. Li, G. Xie, Z. Guo, β-Glucosidase from *Thermotoga naphthophila* RKU-10 for exclusive synthesis of galactotrisaccharides: kinetics and thermodynamics insight into reaction mechanism, Food Chem. 240 (2018) 422–429, https://doi.org/10.1016/j.foodchem.2017.07.155.

[13] M. Hrmova, E.A. MacGregor, P. Biely, R.J. Stewart, G.B. Fincher, Substrate binding and catalytic mechanism of a barley beta-D-Glucosidase/(1,4)-beta-D-glucan exohydrolase, J. Biol. Chem. 273 (1998) 11134–11143, https://doi.org/10.1074/jbc.273.18.11134.

[14] P. Pang, L.-c. Cao, Y.-h. Liu, W. Xie, Z. Wang, Structures of a glucose-tolerant β-glucosidase provide insights into its mechanism, J. Struct. Biol. 2 (2017) 1–9, https://doi.org/10.1016/j.jsb.2017.02.001.

[15] G. Fia, V. Millarini, L. Granchi, G. Bucalossi, S. Guerrini, B. Zanoni, I. Rosi, Beta-glucosidase and esterase activity from *Oenococcus oeni*: screening and evaluation during malolactic fermentation in harsh conditions, LWT- Food Sci. Technol. 89 (2018) 262–268, https://doi.org/10.1016/j.lwt.2017.10.060.

[16] A. Devi, A.K. Aiyappaa, A.L. Waterhouse, Adsorption and biotransformation of anthocyanin glucosides and quercetin glycosides by *Oenococcus oeni* and *Lactobacillus plantarum* in model wine solution, J. Sci. Food Agric. 100 (2020) 2110–2120, https://doi.org/10.1002/jsfa.10234.

[17] J. Zhang, N. Zhao, J. Xu, Y. Qi, X. Wei, M. Fan, Homology analysis of 35 beta-glucosidases in *Oenococcus oeni* and biochemical characterization of a novel beta-glucosidase BGL0224, Food Chem. 334 (2020), 127593, https://doi.org/10.1016/j.foodchem.2020.127593.

[18] M. Dong, M. Fan, Z. Zhang, Y. Xu, A. Li, P. Wang, K. Yang, Purification and characterization of β-glucosidase from *Oenococcus oeni* 31MBR, Eur. Food Res. Technol. 239 (2014) 995–1001, https://doi.org/10.1007/s00217-014-2296-7.

[19] B. Webb, A. Sali, Protein structure modeling with MODELLER, Methods Mol. Biol. 1137 (2014) 1–15, https://doi.org/10.1007/978-1-4939-0366-5_1.

[20] S. Emrah, Y. Sinem, D. Ozkan, T.-B. Dilek, A study of Bos taurus muscle specific enolase; biochemical characterization, homology modelling and investigation of molecular interaction using molecular docking and dynamics simulations, Int. J. Biol. Macromol. 120 (2018) 2346–2353, https://doi.org/10.1016/j.ijbiomac.2018.08.184.

[21] R.A. Laskowski, M.W. MacArthur, J.M. Thornton, PROCHECK validation of protein-structure coordinates, Int. Tables Crystallogr. 21 (2012) 684–687, https://doi.org/10.1107/97809553602060000882.

[22] J.J.P. Stewart, MOPAC: a semiempirical molecular orbital program, J. Comput. Aided Mol. Des. 4 (1990) 1–105, https://doi.org/10.1007/BF00128336.

[23] J.J.P. Stewart, Optimization of parameters for semiempirical methods. III extension of PM3 to Be, Mg, Zn, Ga, Ge, As, Se, Cd, in, Sn, Sb, Te, Hg, Tl, Pb, and Bi, J. Comput. Chem. 12 (1991) 320–341, https://doi.org/10.1002/jcc.540120306.

[24] M.F. Sanner, Python: a programming language for software integration and development, J. Mol. Graph. Model. 17 (1999) 57–61, https://doi.org/10.1016/S1093-3263(99)00019-4.

[25] D.V.D. Spoel, E. Lindahl, B. Hess, G. Groenhof, H.J.C. Berendsen, GROMACS: fast, flexible, and free, J. Comput. Chem. 26 (2005) 1701–1718, https://doi.org/10.1002/jcc.20291.

[26] B. Hess, H. Bekker, H.J.C. Berendsen, J. Fraajie, LINCS: a linear constraint solver for molecular simulations, J. Comput. Chem. 18 (1997) 1463–1472, https://doi.org/10.1002/(SICI)1096-987X.

[27] T. Darden, D. York, L. Pedersen, Particle mesh Ewald: AnN·log(N) method for Ewald sums in large systems, J. Chem. Phys. 98 (1993) 10089–10092, https://doi.org/10.1063/1.464397.

[28] H.J.C. Berendsen, J.P.M. Postma, W.F. van Gunsteren, A. DiNola, J.R. Haak, Molecular dynamics with coupling to an external bath, J. Chem. Phys. 81 (1984) 3684–3690, https://doi.org/10.1063/1.448118.

[29] R. Martonák, A. Laio, M. Parrinello, Predicting crystal structures: the Parrinello-Rahman method revisited, Phys. Rev. Lett. 90 (2003), 075503, https://doi.org/10.1103/PhysRevLett.90.075503.

[30] Q. Dan, W. Xiong, H. Liang, D. Wu, F. Zhan, Y. Chen, S. Ding, B. Li, Characteristic of interaction mechanism between β-lactoglobulin and nobiletin: a multi-spectroscopic, thermodynamics methods and docking study, Food Res. Int. 120 (2019) 255–263, https://doi.org/10.1016/j.foodres.2019.01.003.

[31] N. Shahabadi, M. Maghsudi, Z. Kiani, M. Pourfoulad, Multispectroscopic studies on the interaction of 2-tert-butylhydroquinone (TBHQ), a food additive, with bovine serum albumin, Food Chem. 124 (2011) 1063–1068, https://doi.org/10.1016/j.foodchem.2010.07.079.

[32] M. Totir, N. Echols, M. Nanao, C.L. Gee, A. Moskaleva, S. Gradia, A.T. Iavarone, J. M. Berger, A.P. May, C. Zubieta, Macro-to-micro structural proteomics: native source proteins for high-throughput crystallization, PLoS One 7 (2012), e32498, https://doi.org/10.1371/journal.pone.0032498.

[33] C.J. Gray, B. Schindler, L.G. Migas, M. Pimanová, A.R. Allouche, A.P. Green, S. Mandal, M.S. Motawia, R. Sánchez-Pérez, N. Bjarnholt, Bottom-up elucidation of glycosidic bond stereochemistry, Anal. Chem. 89 (2017) 4540–4549, https://doi.org/10.1021/acs.analchem.6b04998.

[34] M. Gokara, T. Malavath, S.K. Kalangi, R. Pallu, R. Subramanyam, Unraveling the binding mechanism of asiatic acid with human serum albumin and its biological implications, J. Biomol. Struct. Dyn. 32 (2013) 1290–1302, https://doi.org/10.1080/07391102.2013.817953.

[35] R.N. Florindo, V.P. Souza, L.R. Manzine, C.M. Camilo, S.R. Marana, I. Polikarpov, A.S. Nascimento, Structural and biochemical characterization of a GH3 B-glucosidase from the probiotic bacteria *Bifidobacterium adolescentis*, Biochimie 148 (2018) 107–115, https://doi.org/10.1016/j.biochi.2018.03.007.

[36] X. Li, W. Xia, Y. Bai, R. Ma, H. Yang, A novel thermostable GH3 β-Glucosidase from *Talaromyce leycettanus* with broad substrate specificity and significant soybean isoflavone glycosides-hydrolyzing capability, Biomed Res. Int. 2018 (2018) 1–9, https://doi.org/10.1155/2018/4794690.

[37] S. de Ovalle, I. Cavello, B.M. Brena, S. Cavalitto, P. González-Pombo, Production and characterization of a β-glucosidase from *Issatchenkia terricola* and its use for hydrolysis of aromatic precursors in Cabernet Sauvignon wine, LWT- Food Sci. Technol. 87 (2018) 515–522, https://doi.org/10.1016/j.lwt.2017.09.026.

[38] Y. Zhu, H. Jia, M. Xi, L. Xu, S. Wu, X. Li, Purification and characterization of a naringinase from a newly isolated strain of *Bacillus amyloliquefaciens* 11568 suitable for the transformation of flavonoids, Food Chem. 214 (2017) 39–46, https://doi.org/10.1016/j.foodchem.2016.06.108.

[39] D. Leckband, Measuring the forces that control protein interactions, Annu. Rev. Biophys. Biomol. Struct. 29 (2000) 1–26.

[40] C.A.M. Seidel, A. Schulz, M.H.M. Sauer, Nucleobase-specific quenching of fluorescent dyes. 1. Nucleobase one-electron redox potentials and their correlation with static and dynamic quenching efficiencies, J. Phys. Chem. 100 (1996) 5541–5553, https://doi.org/10.1021/jp951507c.

[41] J.L. Liu, Y.C. Kong, J.Y. Miao, X.Y. Mei, S.Y. Wu, Y.C. Yan, X.Y. Cao, Spectroscopy and molecular docking analysis reveal structural specificity of flavonoids in the inhibition of alpha-glucosidase activity, Int. J. Biol. Macromol. 152 (2020) 981–989, https://doi.org/10.1016/j.ijbiomac.2019.10.184.

[42] J.N. Varghese, M. Hrmova, G.B. Fincher, Three-dimensional structure of a barley b-D-glucan exohydrolase, a family 3 glycosyl hydrolase, Structure 7 (1999) 179–190, https://doi.org/10.1016/S0969-2126(99)80024-0.

[43] H. Gammadde, P. Pilimathalawe, V. Naduviladath, S. Mahindagoda, L. Ravindra, S. Wijepurage, *Trichoderma virens* β-glucosidase I (BGLI) gene; expression in *Saccharomyces cerevisiae* including docking and molecular dynamics studies, BMC Microbiol. 17 (2017), https://doi.org/10.1186/s12866-017-1049-8.

[44] S.R. Dodda, A. Aich, N. Sarkar, P. Jain, S. Jain, S. Mondal, K. Aikat, S. S. Mukhopadhyay, Structural and functional insights of β-glucosidases identified from the genome of *Aspergillus fumigatus*, J. Mol. Struct. 1156 (2018) 105–114, https://doi.org/10.1016/j.molstruc.2017.11.078.

[45] K.Y. Li, J. Jiang, M.D. Witte, W.W. Kallemeijn, W.E. Donker-Koopman, R.G. Boot, J.M.F.G. Aerts, J.D.C. Codée, Gijsbert A. d. M. Van, H.S. Overkleeft, Exploring functional cyclophellitol analogues as human retaining beta-glucosidase inhibitors, Org. Biomol. Chem. 12 (2014) 7786–7791, https://doi.org/10.1039/c4ob01611d.

[46] A.I. Guce, N.E. Clark, E.N. Salgado, D.R. Ivanen, A.A. Kulminskaya, H. Brumer, S. C. Garman, Catalytic mechanism of human alpha-galactosidase, J. Biol. Chem. 285 (2010) 3625–3632, https://doi.org/10.1074/jbc.M109.060145.